

# The extended X–ray emission around RRAT J1819–1458

A. Camero-Arranz<sup>1\*</sup>, N. Rea<sup>1</sup>, N. Bucciantini<sup>2,3</sup>, M. A. McLaughlin<sup>4</sup>, P. Slane<sup>5</sup>,  
 B. M. Gaensler<sup>6</sup>, D. F. Torres<sup>1,7</sup>, L. Stella<sup>8</sup>, E. de Oña<sup>1</sup>, G. L. Israel<sup>8</sup>, F. Camilo<sup>9,10</sup>  
 and A. Possenti<sup>11</sup>

<sup>1</sup> Institut de Ciències de l’Espai, (IEEC-CSIC), Campus UAB, Fac. de Ciències, Torre C5, parell, 2a planta, 08193 Barcelona, Spain

<sup>2</sup> INAF - Osservatorio Astrofisico di Arcetri, L.go E. Fermi 5, 50125, Firenze, Italy

<sup>3</sup> INFN - Sezione di Firenze, Via G. Sansone 1, 50019 Sesto Fiorentino, Firenze, Italy

<sup>4</sup> Department of Physics, West Virginia University, Morgantown, WV 26501, USA

<sup>5</sup> Harvard-Smithsonian Center for Astrophysics, 60 Garden St. Cambridge, MA 02138, USA

<sup>6</sup> The University of Sydney, Room 216, 44 Rosehill Street, Redfern, NSW 2016, Australia

<sup>7</sup> Institució Catalana de Recerca i Estudis Avançats (ICREA)

<sup>8</sup> INAF - Osservatorio Astronomico di Roma, Via Frascati 33, I-00040 Monteporzio Catone (Roma), Italy

<sup>9</sup> Columbia Astrophysics Lab, Columbia University, New York, NY 10027, USA

<sup>10</sup> Arecibo Observatory, HC3 Box 53995, Arecibo, PR 00612, USA

<sup>11</sup> INAF-Osservatorio Astronomico di Cagliari, loc. Poggio dei Pini, strada 54, 09012 Capoterra, Italy

13 November 2017

## ABSTRACT

We present new imaging and spectral analysis of the recently discovered extended X–ray emission around the high magnetic field rotating radio transient RRAT J1819–1458. We used two *Chandra* observations performed for this object in 2008 May 31 and 2011 May 28, respectively. The diffuse X–ray emission was detected with a significance of  $\sim 19\sigma$  in the image obtained by combining the two observations. Neither long-term spectral nor timing variability have been observed from the source or the nebula. RRAT J1819–1458 shows an unusual high X–ray efficiency of  $\eta_X \equiv L_{X(0.3-5\text{ keV})}/\dot{E}_{rot} \sim 0.15$  at converting spin-down power into X–ray luminosity. The most favourable scenario for the origin of this extended X–ray emission is either a pulsar-wind nebula (PWN) or a scattering halo. A magnetically powered scenario for the extended emission is viable only in the case of a Compton nebula, while can be tentatively disfavoured in the case of synchrotron emission.

**Key words:** pulsars: individual (RRAT J1819–1458)—stars: magnetic fields—stars: neutron—X–rays: stars

## 1 INTRODUCTION

Rotating Radio Transients (RRATs) are radio pulsars that were discovered through their sporadic radio bursts (McLaughlin et al. 2006). There are  $\sim 70$  currently known RRATs, with spin periods ranging from 0.1 to 7 s (Keane and McLaughlin 2011, and references therein).

At a radio frequency of 1.4 GHz, radio bursts are observed from RRAT J1819–1458 roughly every  $\sim 3$  minutes with the Parkes telescope. The spin period of RRAT J1819–1458 is 4.3 s ( $\dot{P} \sim 3.2 \times 10^{-13} \text{ s s}^{-1}$ ; Lyne et al. 2009), with a characteristic age of 117 kyr and a dipolar magnetic field of  $B \sim 5 \times 10^{13}$  G. The spin-down energy loss rate measured for this source is  $\dot{E}_{rot} \sim 3 \times 10^{32} \text{ erg s}^{-1}$ . Two glitches have

been detected, with one of these showing anomalous post-glitch recovery that suggests RRAT J1819–1458 originated in the magnetar region of the period-period derivative diagram (Lyne et al. 2009).

RRAT J1819–1458 is the only source of this type also detected at X–rays energies so far (Reynolds et al. 2006; McLaughlin et al. 2007; Rea et al. 2008; Kaplan et al. 2009). The distance inferred from its dispersion measure ( $196 \pm 3 \text{ pc cm}^{-3}$ ) is 3.6 kpc, with at least a 25% of uncertainty (McLaughlin et al. 2007, and references therein). The spectrum of RRAT J1819–1458 is well modeled by an absorbed blackbody ( $N_H \sim 6 \times 10^{21} \text{ cm}^{-2}$  and  $kT \sim 0.14 \text{ keV}$ ) with a broad spectral absorption line at  $\sim 1 \text{ keV}$  (McLaughlin et al. 2007, Rea et al. 2009). The X–ray luminosity is  $L_X \sim 4 \times 10^{33} (\text{d}/3.6 \text{ kpc})^2 \text{ erg s}^{-1}$ , more than one order of magnitude higher than the spin-down luminosity.

\* E-mail: camero@ice.cat

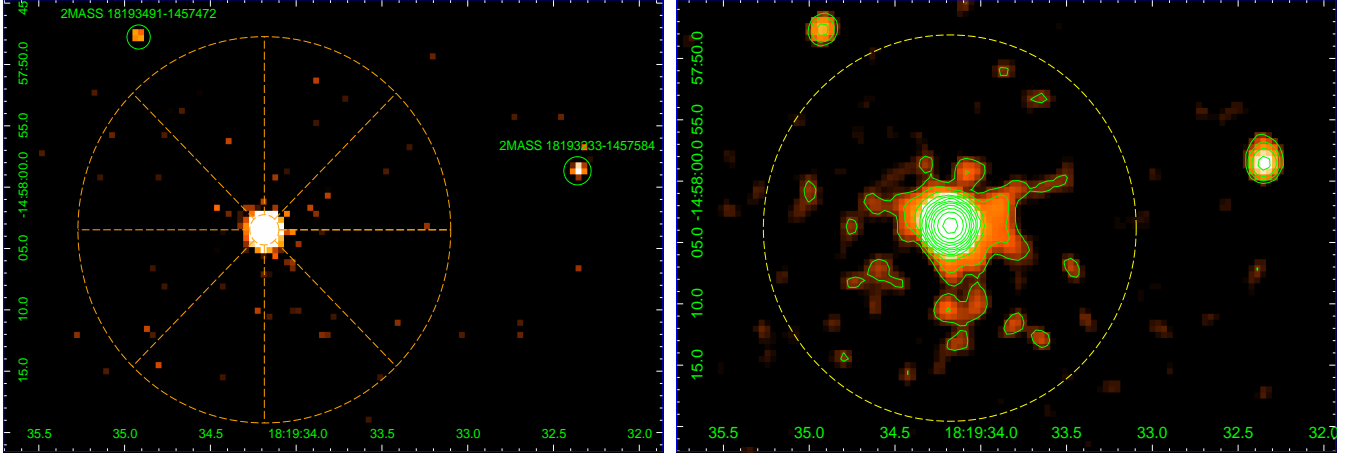


**Figure 1.** *Left panel:* Combined 0.3–10 keV log image of RRAT J1819–1458, using both *Chandra* ACIS-S observations from 2008 and 2011, with a panda region of outer radius  $16''$  and inner radius  $5''$  overplotted. The offsets from the RRAT J1819–1458 position are  $\sim 19''$  and  $\sim 27''$  for the 2MASS 18193491–1457472 and 18193233–1457584 sources, respectively. *Right panel.* Smoothed image using a Gaussian function with a radius of 3 pixels and with  $3\sigma$  contours of the extended emission and a circular region of  $16''$  overplotted. Colors are proportional to the log of the X-ray intensity. North is up, and east is to the left. One ACIS-S pixel corresponds to  $0''.492$ .

Diffuse X-ray emission was found around RRAT J1819–1458 in a  $\sim 30$  ks *Chandra* observation carried out in 2008, with a luminosity of  $\sim 10^{32}$  erg s $^{-1}$  and extending to  $\sim 13''$  from the source (Rea et al. 2009). Furthermore, the pulsar’s error circle was refined performing a boresite correction of this new *Chandra* observation, using a 2MASS field star present in both X-ray and infrared images. This resulted in an accurate position of right ascension  $\alpha = 18^{\text{h}}19^{\text{m}}34^{\text{s}}.173$  and declination  $\delta = -14^{\circ}58'03''.57$  (J2000; with a  $1\sigma$  error of  $\sim 0.3''$  in both coordinates; Rea et al. 2009).

So far there is no evidence of an optical counterpart for RRAT J1819–1458 (see e.g. Dhillon et al. 2011). However, near-infrared observations (J, H and Ks filters) resulted in the identification of a possible candidate near-infrared counterpart which is the only source within the  $1\sigma$  X-ray positional error circle (Rea et al. 2010).

In this work, we present the study resulting from the reduction and combined analysis of two *Chandra* observations for RRAT J1819–1458, performed on 2008 May 31 (Rea et al. 2009) and 2011 May 28 (this work). Observations and data reduction are reported in Section 2, the analysis and results in Section 3, and a discussion in Section 4.

## 2 OBSERVATIONS AND DATA REDUCTION

The *Chandra* X-ray Observatory observed RRAT J1819–1458 with the Advanced CCD Imaging Spectrometer (ACIS) instrument on 2008 May 31 (ObsID 7645) for 30 ks and again in 2011 May 28 (ObsID 12670) for 90 ks, both in VERY FAINT (VF) timed exposure imaging mode.

For both observations, we used a 1/8 subarray, which provides a time resolution of 0.4 s, and the typical ACIS-S imaging and spectral configurations. The source was positioned in the back-illuminated ACIS-S3 CCD at the nominal target position. Standard processing of the data was performed by the *Chandra* X-ray Center to Level 1 and Level 2 (processing software DS 7.6.11.6 for ObsID 7645 and 8.4.3 for ObsID 12670).

In this work we have used CIAO software (ver. 4.4) for the posterior processing and analysis of the data, resulting in a final exposure time of 27.88 ks for the first observation and 80.40 ks for the second one.

## 3 ANALYSIS AND RESULTS

### 3.1 Imaging

To study the extended X-ray emission found by (Rea et al. 2009) in more detail, we proceeded with the extraction of a combined image in the 0.3–10 keV energy range, using the two *Chandra* observations described in the previous Section. Before merging the two observations, we reprojected the events onto the same tangent plane. Therefore, for aligning and merging event files from different ObsIDs we used the CIAO tool `reproject_image`. Figure 1 shows the resultant combined image where diffuse extended X-ray emission is clearly visible around the compact object.

We applied the CIAO `wavdetect` tool to the  $\sim 90$  ks ACIS-S cleaned image and found RRAT J1819–1458 at  $\alpha = 18^{\text{h}}19^{\text{m}}34.178^{\text{s}}$  and  $\delta = -14^{\circ}58'03''.662$  (J2000), with a statistical error of  $0''.007$  radius, and 2 X-ray bright stars in the field detected at a significance of  $>5\sigma$ . The second star detected is the Two Micron All Sky Survey (2MASS)<sup>1</sup> star 18193233–1457584 at  $\alpha = 18^{\text{h}}19^{\text{m}}32.34^{\text{s}}$  and  $\delta = -14^{\circ}57'58''.68$  (J2000), with an accuracy of  $0''.07$  radius (catalog position:  $\alpha = 18^{\text{h}}19^{\text{m}}32.34^{\text{s}}$  and  $\delta = -14^{\circ}57'58''.41$ , with an accuracy of  $0''.08$  radius (see also Rea et al. 2009).

The third source detected, at  $\alpha = 18^{\text{h}}19^{\text{m}}34.92^{\text{s}}$  and  $\delta = -14^{\circ}57'47''.68$  (statistical error of  $0''.12$  radius), was consistent with the 2MASS star 18193491–1457472 (catalog position of  $\alpha = 18^{\text{h}}19^{\text{m}}34.912^{\text{s}}$  and  $\delta = -14^{\circ}57'47''.22$ , with a  $0''.11$  error radius). We then proceeded to perform a bore-site correction of the field to refine the

<sup>1</sup> <http://www.ipac.caltech.edu/2mass>

RRAT J1819-1458 position and error circle. Assuming a physical association between the 2MASS stars and their coincident X-ray sources, the final RRAT J1819-1458 position is  $\alpha = 18^{\text{h}}19^{\text{m}}34.18^{\text{s}}$  and  $\delta = -14^{\circ}58'03''.7$ , with a  $1\sigma$  associated error circle of  $0''.2$  radius (computed doing a quadratic mean of all the positional and statistical errors plus the 2MASS catalog intrinsic systematic errors).

### 3.2 Timing

For the timing analysis, we first referred the arrival time of each photon to the barycenter of the solar system using the CIAO tool `axbary`. Then, we used the `dmextract` tool to create background-subtracted lightcurves, using the time resolution of the data ( $\sim 0.4$  s). For this, we extracted the source photons on each individual observation from a circular region with  $2''.5$  radius, and another one for the background, far from the source.

Using the `Xronos` package, we folded both X-ray data sets using the radio ephemeris (Lyne et al. 2009), confirming the sinusoidal X-ray modulation found with *XMM-Newton* (McLaughlin et al. 2007) and *Chandra* (Rea et al. 2009). In addition, we performed a periodicity search obtaining a  $P_{\text{spin}} = 4.26328(6)$  s (epoch = MJD 54617), in agreement with previous work. The 0.3–5 keV pulsed fraction for the new *Chandra* observation (ObsID 12670) was of  $31 \pm 4\%$ , defined as  $(F_{\text{max}} - F_{\text{min}})/(F_{\text{max}} + F_{\text{min}})$ , with  $F_{\text{max}}$  and  $F_{\text{min}}$  the maximum and minimum counts of the background-corrected X-ray pulse profile. The shape of the pulse profile, and the pulsed fraction, are consistent with past measurements (Reynolds et al. 2006; McLaughlin et al. 2007; Rea et al. 2009), showing no evidence for long-term variability.

### 3.3 Spectroscopy

#### 3.3.1 RRAT J1819–1458

We used the `specextract` script, which uses a combination of CIAO tools, to extract source and background spectra for a point-like ACIS source like RRAT J1819–1458. To extract only the photons from the point source for both observations, a circular region with  $2''.5$  radius and a circular background region of radii  $18''$  (far from the source) were used. We neglected in the source spectral analysis the projected emission from the extended X-ray nebula since it only contributed  $\sim 3\%$  of the counts. The point source spectrum was rebinned so as to have at least 25 counts per spectral bin, so that  $\chi^2$  statistics could be used.

We modeled each spectrum using the XSPEC v.12.7.0u analysis package. Following previous studies (McLaughlin et al. 2007; Rea et al. 2009), we fit the continuum of each spectrum with an absorbed blackbody. However, a single blackbody fit does not represent the spectrum properly ( $\chi_r^2 \sim 1.7$ ; 47 dof). We added to that model the previously detected absorption line at 1 keV (McLaughlin et al. 2007; Rea et al. 2009), which we modeled with a Gaussian function (`phabs*bbbodyrad*gabs` in XSPEC notation). Table 3.1 shows the spectral parameters obtained for the best fit. Since the Hydrogen absorption column was not found to

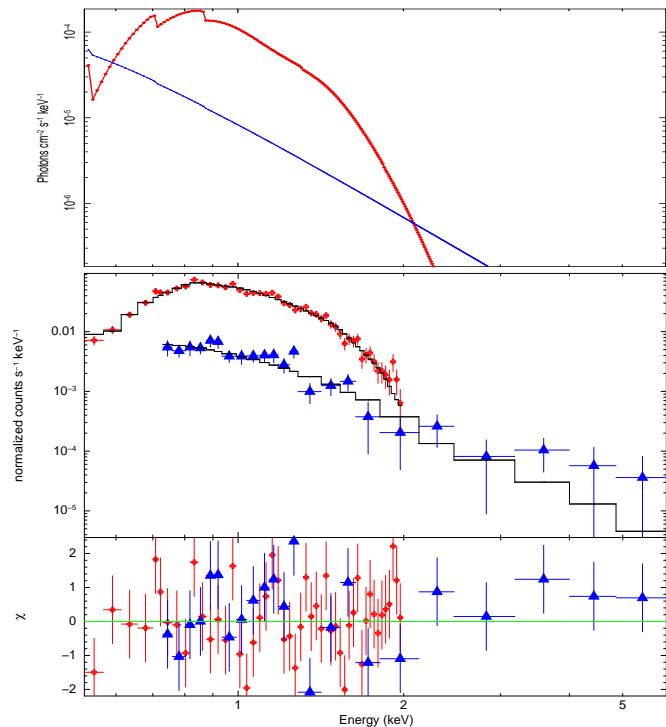


**Figure 2.** Best-fit deconvolved model (top panel) for RRAT J1819–1458 (red circles) and the extended X-ray emission (blue triangles). The spectrum of RRAT J1819–1458 was modeled with an absorbed blackbody plus a  $\sim 1$  keV absorption line, and an absorbed power-law for the extended X-ray emission. The normalized spectra and residuals are also shown in the middle and bottom panels, respectively.

significantly vary between observations, we fixed this parameter in both observations at the value found by McLaughlin et al. (2007) using an *XMM-Newton* observation. This allowed us to better constrain the 1 keV feature with respect to the previous *Chandra* observation, although it is not as well resolved as with the *XMM-Newton* observation (Miller et al. 2012 in preparation), due to the different effective area of the two satellites. The inferred blackbody radius is  $14 \pm 8$  km, assuming a 3.6 kpc distance.

In order to increase the signal to noise of the spectrum we proceeded to combine the spectra created for ObsID 7645 and 12670 and associated responses. For this we used the CIAO tool `combine_spectra` and then we rebinned the final  $\sim 0.5$ –2 keV combined spectrum to have at least 25 counts per spectral bin (see Figure 2). We used in addition the FTOOL `mathpha`, yielding similar results. Once again, the combined spectrum was modeled in XSPEC with the same model as before (see Table 3.1). Fitting the two individual spectra simultaneously with the same model also yielded similar results.

In the new *Chandra* observation (ObsID 12670), the point source RRAT J1819–1458 has an ACIS-S 0.3–10 keV count rate of  $0.0374(7)$  counts  $\text{s}^{-1}$  (background subtracted)

**Table 1.** Best-Fit Spectral Parameters<sup>a</sup>.

ObsID	RRAT J1819–1458			Flux <sup>e</sup>	$\chi_r^2(\text{DOF})$	DIFFUSE EMISSION			$\chi_r^2(\text{DOF})$
	$N_{\text{H}}^b$	$T_{\text{BBODY}}^c$ <i>norm</i> <sup>d</sup>	$E_{\text{gauss}}^c$ $\sigma^c$			$N_{\text{H}}^b$	$\alpha$ <i>norm</i> <sup>f</sup>	Flux <sup>e</sup>	
7645 (May 2008)	0.6 (fixed)	0.129±0.003 1600 <sup>+300</sup> <sub>-200</sub>	1.13±0.04 0.14±0.05	1.37 ±0.05	1.05(29)	<0.7	3.6±0.4 10.3±0.2	0.22±0.04	1.01(6)
12670 (May 2011)	0.6 (fixed)	0.129±0.002 1400 <sup>+200</sup> <sub>-100</sub>	1.16±0.03 0.17±0.04	1.30±0.02	1.30(44)	<0.7	3.5±0.3 9.7±0.8	0.25±0.04	1.10(17)
7645+12670 (combined)	0.6 (fixed)	0.130±0.002 1500±100	1.16±0.03 0.17±0.03	1.35±0.02	1.10(45)	<0.9	3.7±0.3 8.7±0.6	0.23±0.02	1.26(19)

<sup>a</sup>Results of the spectral modeling with a `phabs*bbbodyrad*gabs` and `phabs*power`, for source and diffuse emission, respectively;

<sup>b</sup>All errors are at 90% confidence level;  $N_{\text{H}}$  in units of  $10^{22} \text{ cm}^{-2}$ ;

<sup>c</sup>Gaussian absorption line energy and width in keV units;

<sup>d</sup>a constant of value  $R_{km}^2/d_{10}^2$ , where  $R_{km}$  is the source radius (km) and  $d_{10}$  is the distance in units of 10 kpc;

<sup>e</sup>absorbed flux in units of  $\times 10^{-13} \text{ erg cm}^{-2} \text{ s}^{-1}$  (0.3–5 keV);

<sup>f</sup> Photon Index with normalization units in  $10^{-6} \text{ photons keV}^{-1} \text{ cm}^{-2} \text{ s}^{-1}$  at 1 keV.

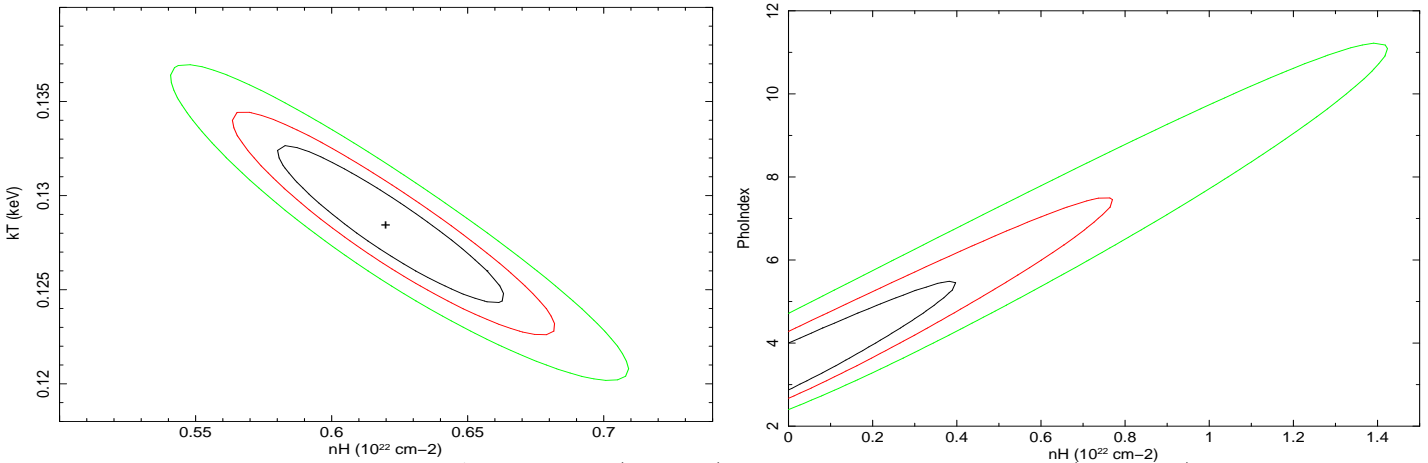


**Figure 3.** Confidence contours for RRAT J1819–1458 (left panel) and the extended X–ray emission (right panel) in the  $N_{\text{H}} - kT$  and  $N_{\text{H}} - \text{Gamma}$  spaces, respectively. From inside to outside  $1\sigma$ ,  $2\sigma$ , and  $3\sigma$  contours are displayed.

and in the combined observation the count rate is 0.0391(6) counts  $\text{s}^{-1}$  (a total of  $\sim 4225$  counts).

### 3.3.2 The diffuse X–ray emission

To extract the photons from the diffuse X–ray emission for both observations, we followed the same procedure as in Rea et al. (2009) and selected an annular region of inner radius  $2''.5$  and outer radius of  $20''$ , to ensure that the whole extended X–ray emission was included (see Fig. 1 and Sect. 3.4). For the background we selected a similar annular region but far from the extended X–ray emission. An absorbed power law provides a good fit to the data (see Ta-

ble 3.1; the spectrum was grouped with at least 25 counts per bin), but the spectral parameters are somewhat poorly determined due to the small number of counts (see also Rea et al. 2009).

Following the same approach as for RRAT J1819–1458, we then create a combined spectrum using `combine_spectra` (see previous Section). Figure 2 shows the obtained combined  $\sim 0.8\text{--}7$  keV spectrum for the extended source (the spectrum was also grouped with at least 25 counts per bin). The background contribution is  $\sim 35\%$  for the extended emission. The extended X–ray emission has a 0.3–10 keV count rate of 0.0077(5) counts  $\text{s}^{-1}$  (background subtracted) and a total of  $\sim 830$  counts. In Table 3.1 we display the spec-

tral parameters resulted from the best fitting for all the spectra. We note that fixing the Hydrogen absorption column to the pulsar’s value showed systematic departures from the data at high energies, preventing us from constraining the rest of the parameters. This is an effect of poor statistics, with the limits of the  $N_H$  derived for the nebula being consistent with the value obtained for the point source (see Fig. 3.3.1).

### 3.4 The diffuse X-ray emission structure

To infer the significance and estimate the luminosity of the whole diffuse emission in the combined image, we built the combined Chart/MARX point-spread function (PSF). To do this, we first built a Chart/MARX PSF for each individual observation, using both the RRAT J1819–1458 spectrum and its corresponding exposure time. The CIAO tool `reproject_image` then reprojected the events onto the same tangent plane, and created a final combined PSF image.

In Figure 1, we compare the surface brightness radial distribution of the combined Chandra observation of RRAT J1819–1458 with that of the combined Chart/MARX PSF plus a background level. Both surface brightnesses were obtained by extracting counts from 50 annular regions (each 2 pixels wide) centered on the source position, and for the RRAT J1819–1458 one, after removal of the serendipitous point sources in the field. This figure shows that the extended emission becomes detectable around 5 pixels ( $\sim 2''.5$ ) from the peak of the source PSF.

To compute the significance of the diffuse X-ray emission around RRAT J1819–1458, from the combined image we extracted all the photons from an annular region of  $2''.5$ – $20''$  radii, and we subtracted from it the background extracted from a similar region far from the source (but in the same S3 CCD). This resulted in an excess of  $790 \pm 18$  counts, which corresponds to a detection significance of  $\sim 19\sigma$ .

Finally, we studied any possible change in the morphology of the extended X-ray emission between the 2008 and 2011 observations. To account for this we applied the Kolmogorov-Smirnov statistic (KSTWO), using the count-rate/pixel<sup>2</sup> from each surface brightness radial distributions as input vectors, to study whether the two images were drawn from the same distribution. The associated probability resulted to be  $\sim 0.7$ , meaning that the two data sets most likely come from the same distribution. In addition, we did not find in the combined image any azimuthal asymmetry in the diffuse emission (see right panel of Fig. 1).

## 4 DISCUSSION

In the present work we have not found long-term variability in spectral and timing X-ray properties for RRAT J1819–1458. The spectral continuum for the point source was well fitted with an absorbed blackbody model, in good agreement with previous results (McLaughlin et al. 2007; Rea et al. 2009). The previously reported absorption line at 1 keV (McLaughlin et al. 2007; Rea et al. 2009) is visible in all the observations. For the extended X-ray emission the spectral parameters did not change in time, and are compatible with the result from Rea et al. (2009). In addition, the diffuse X-ray emission was detected in the combined image with a

significance of  $\sim 19\sigma$ , substantially improving the detection level reported in its discovery (Rea et al. 2009).

The energies of pulsar wind electrons and positrons range from  $\sim 1$  GeV to  $\sim 1$  PeV, placing their synchrotron and inverse Compton emission into radio–X-ray and GeV–TeV bands, respectively. This multi-wavelength emission can be seen as a pulsar-wind nebula (Kargaltsev et al. 2012, and references therein). To date, the exact physical origin and acceleration mechanism of the high-energy particles in the pulsar winds are poorly understood, and not all nebulae can be easily explained as spin-down-powered PWNe.

In Rea et al. (2009) we discussed different scenarios for the origin of the extended emission detected around RRAT J1819–1458. One option was that the extended emission we observe is part of the remnant of the supernova explosion which formed RRAT J1819–1458, unlikely for an object of 117 kyr. Another possibility was a bow-shock nebula due to the pulsar moving supersonically through the ambient medium, but this was ruled out since the projected velocity in the case of a bow shock would be rather small ( $v_p \sim 20$  km s<sup>−1</sup>; see Rea et al. 2009 and references therein).

Other possibilities are that RRAT J1819–1458 could power a sort of PWN, or the extended X-ray emission around the pulsar might be explained as a magnetic nebula, or as a scattering halo as for 1E 1547–5408 (Vink and Bamba 2009; Olausen et al. 2011) and Swift J1834.9–0846 (Younes et al. 2012; Esposito et al. 2012).

In the following we will investigate the PWN hypothesis for the extended emission found in coincidence with RRAT J1819–1548. This is mostly a qualitative analysis, trying to constrain a possible PWN interpretation. A distance of 3.6 kpc is assumed. At that distance the observed diffuse emission extending to  $20''$  corresponds to a radius of the nebula:  $R_{\text{pwn}} \approx 1$  ly. X-ray PWNe are usually observed in coincidence with young pulsars ( $\tau \sim 10^{3-4}$  yr), which have high spin-down luminosity to power the observed emission. Their X-ray luminosity in the 2–10 keV band is found to positively correlate (Li et al. 2008) with the spin-down power  $\dot{E}$  (more energetic pulsars tend to inject more high energy particles). The X-ray luminosity is also found to anticorrelate with the characteristic age  $\tau$  (older systems tend to be less compact and with a lower magnetic field). However, we caveat that in the latter correlations there could be important selection effects, as well as a scatter by several orders-of-magnitude.

For the nebula associated with RRAT J1819–1548, extrapolating the observed flux and using the observed photon index, we find  $L_X[2-10 \text{ keV}] \sim 1.5 \times 10^{30} \text{ erg s}^{-1} \pm 50\%$ , while the correlations found by Li et al. (2008), with  $\dot{E} \sim 3 \times 10^{32} \text{ erg s}^{-1}$  would result in  $L_X = 3.1 \times 10^{27} \text{ erg s}^{-1}$ . It is evident that compared with other pulsars showing PWNe, this nebula show a relatively high efficiency in converting rotational energy in X-ray luminosity.

However the relations in Li et al. (2008), derived for young and energetic pulsars, when extrapolated to low values of  $\dot{E}$ , typical for RRAT J1819–1548, have large uncertainties. Thus the inferred value for  $L_X$  with respect to our measured value, despite a few orders of magnitude difference, is compatible within a couple of standard deviations of the model predictions (Li et al. 2008).

Another peculiar aspect of the detected extended X–

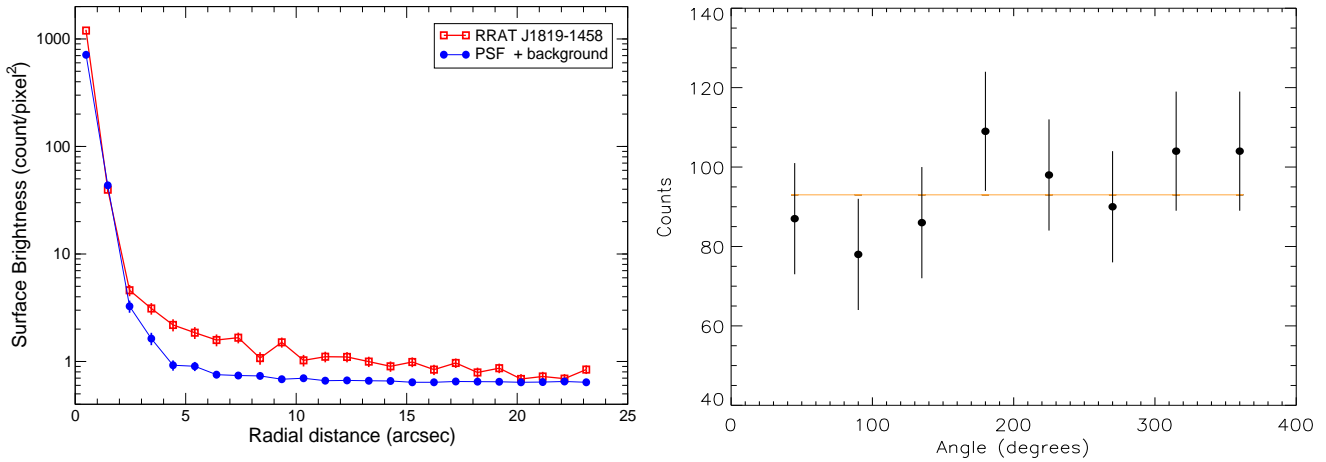


**Figure 4.** *Left.* Surface brightness of the background-subtracted ACIS-S image of RRAT J1819–1458 (red open squares) and of the Chart/MARX PSF plus a constant background (blue circles). *Right.* Azimuthal distribution of counts (background subtracted) in the extended X–ray emission for a panda region divided in 8 sections (see left panel of Fig. 1; West, to the right, corresponds to 0 degrees, with the angle increasing counterclockwise). A constant fit is overplotted (reduced  $\chi^2 \sim 0.7$ ; constant  $\sim 94$  counts).

ray emission is the very steep photon index  $\Gamma_{\text{pwn}}$ . If one assumes an injection spectrum of X–ray emitting particles  $\dot{N}(E) \propto E^{-p}$  one gets for the photon index:  $(p+1)/2 < \Gamma_{\text{pwn}} < (p+2)/2$  (Pacini and Salvati 1973). In the following discussion we will assume that the synchrotron cooling time of X–ray emitting particles is shorter than the age of the nebula. Synchrotron cooling timescale for X–ray emitting particles in magnetic fields of  $\sim 10\mu\text{G}$  (see the discussion below on the possible values of the magnetic field), are much smaller than the spin-down age of the system. Therefore, an injection spectrum with  $p = 5$  is needed to explain the observed photon index, while typical values in other PWNe are found to be  $p \sim 2.1 - 2.5$ . RRAT J1819–1548, with  $L_X[0.3-5\text{keV}] = 3.6 \times 10^{31}\text{erg s}^{-1} \sim 0.12 \times \dot{E}$ , would have to inject  $> 12\%$  of the total spin-down power in the form of X–ray emitting particles. Given the steep photon spectrum that we observe, the X–ray efficiency (12%) with respect to  $\dot{E}$  is insensitive to our choice for the high energy limit of the energy band (5 keV). However it is very sensitive to the low energy limit (0.3 keV). This suggests that the observed photon spectrum cannot extend smoothly below this energy, otherwise the total efficiency could rapidly exceed 100%. We will assume in the following discussion that a spectral break is present at 0.3 keV.

Let us now attempt to build a standard PWN model, and see if, and under which conditions (limits) the observed properties can be reproduced. We want to stress here, that given the paucity of data (only an X–ray flux and photon index are available) and the uncertainties in our assumptions (for example the distance), this is mostly an attempt to constrain the plausibility of a PWN interpretation. In general the pulsar wind will inject into the nebula both relativistic particles and magnetic field:  $\dot{E} = \dot{E}_{\text{part}} + \dot{E}_{\text{mag}}$  (with  $\dot{E}_{\text{part}}$  being the energy injected in particles and  $\dot{E}_{\text{mag}}$  the energy injected in magnetic field). It is found that, in many PWNe, a single power-law injection spectrum for the particles cannot reproduce the observed integrated spectra

from radio to X–rays. To fit the integrated broad band spectrum, one requires the injected particles to have at least an energy distribution in the form of a broken power-law (Bucciantini et al. 2011). If we call  $E_b$  the break energy, then the injection spectrum of the particles is:

$$\dot{N}(E < E_b) \propto (E/E_b)^{-\alpha_1}, \quad (1)$$

$$\dot{N}(E > E_b) \propto (E/E_b)^{-\alpha_2}. \quad (2)$$

From the observed X–ray photon index, we can fix the high energy slope of the injected spectrum  $\alpha_2 = 5$ . For the low energy part one can adopt the flattest value measured in PWNe in radio,  $\alpha_1 = 1$ . We stress here that for the following discussion, this is the most optimistic assumption, that minimizes the amount of energy injected below the break  $E_b$ . The energy injected in particles is:

$$\dot{E}_{\text{part}} = \int_0^\infty E \dot{N}(E) dE. \quad (3)$$

On the other hand, the energy injected above the break is

$$\dot{E}_{\text{part}}(E > E_b) = \int_{E_b}^\infty E \dot{N}(E) dE \approx 0.25 \dot{E}_{\text{part}}. \quad (4)$$

Thus of all the energy injected in particles, for our values of  $\alpha_1$  and  $\alpha_2$ ,  $\sim 25\%$  is in particles with  $E > E_b$  (above the break). Of course this number can be further increased if one introduces a low energy cutoff, which however is not observed in other PWNe, or if a smooth break is assumed. Taking into account the synchrotron cooling and the inferred injection spectrum at high energy, one can show that in order to have a  $\sim 12\%$  efficiency in the radiated X–rays, as observed, one needs to inject  $\sim 25 - 30\%$  of the total spin-down power in the form of X–ray emitting particles.

We will call  $E[\nu_X]$  the energy of particles responsible for the emission photons with energy  $\nu_X$ . For the synchrotron emission the value of this energy is a function of the energy of the emitted photon and of the magnetic field. Despite the fact that the magnetic field is not known, we will show



that information on the inferred injection spectrum, can be used to constrain it. Taking into account all that was stated before, we conclude that:

- $E_b$  cannot be  $\gg E[0.3\text{keV}]$ , otherwise we would get a harder spectrum than the one observed.
- $E_b$  cannot be  $\ll E[0.3\text{keV}]$ , otherwise the fraction of energy injected in X-ray emitting particles would be  $<25\%$  of  $\dot{E}_{part}$  and  $<25\%$   $\dot{E}$  (and we could not explain the high X-ray efficiency).

Using the above constraints we can put an upper limit on the value of the nebular magnetic field. Assuming  $E_b \approx E[0.3\text{keV}]$ , and recalling that 25% of the energy must be injected above the break, we find that almost 75% of the total spin-down energy is injected in particles below the break. This implies that  $\dot{E}_{mag} \ll \dot{E}$ , i.e. the high X-ray efficiency requires that most of the energy is injected into particles, with little left to be injected into the magnetic field. The magnetic energy content of the nebula is  $E_{mag} \sim \dot{E}_{mag} \times \tau \sim \eta_B \times \dot{E} \times \tau$ , where  $\eta_B$  can be roughly assumed  $<0.1$ , which gives a magnetic field  $B_{pwn} < 20\mu\text{G}$ . On the other hand, we can show that  $B$  must be greater than  $\sim 1\mu\text{G}$ . In fact if  $B$  was  $\leq 1\mu\text{G}$ , then assuming synchrotron radiation, the energy of particles emitting at  $\sim 1\text{keV}$  would have to be  $E[1\text{keV}] \geq 5 \times 10^{13}\text{eV}$ , while the particles energy associated with the voltage drop ( $\Phi$ ) of the pulsar, is only  $5 \times 10^{13}\text{eV}$ , and a PWN can accelerate only a negligible fraction of particles beyond this energy. The observation of a bright X-ray nebula suggests that this cannot be the case. Despite this value of the magnetic field being smaller than typical values in the ISM we want to recall here that the PWN is not expanding in the ISM but inside the SNR ejecta (not to be confused with the SNR shell), whose magnetic field can in principle be much smaller. One can also compute the value of the equipartition magnetic field. Given that most of the energy is injected in particles emitting in the soft-X-rays, equipartition must be computed with respect to them. The value for the equipartition magnetic field is found to be  $B_{pwn-eq} \sim 7 - 10\mu\text{G}$ . Interestingly, such value is compatible with the two limits we found before. This suggests that, in the hypothesis of a synchrotron nebula, the magnetic field should then be in the range of a few– $20\mu\text{G}$ .

Summarizing, this study shows that to explain the observed extended X-ray emission as a PWN:

- (i) Most of the spin-down energy must be injected in particles.
- (ii) A large fraction (25 – 30%) of the spin-down energy must be injected in particles emitting in the soft X-ray/EUV ( $E_b = E[0.3\text{keV}]$ ).
- (iii) The magnetic field in the nebula,  $B_{pwn}$ , must be  $< 20\mu\text{G}$ , otherwise there would be little energy left in the particles to explain the observed X-ray efficiency.
- (iv)  $B_{pwn}$  must be  $> 1\mu\text{G}$ , otherwise one would need a large amount of particles with energies above the one given by the pulsar voltage drop  $\Phi$  to explain the X-ray emission.
- (v)  $E[1\text{keV}] \sim e\Phi$ , the energy related to pulsar voltage drop. This might explain the steep X-ray spectrum, with the X-ray emitting particles having energies close to the high-energy cutoff.

The above model was developed, assuming a standard PWN interpretation of the observed emission, where X-ray

are due to synchrotron. However it is also possible that we are observing a Compton nebula, where the X-ray emission is due to Inverse Compton on the CMB, by a relic electron population with typical energies  $\sim 1\text{GeV}$ . For a magnetic field in the nebula  $B_{pwn}$  one would then expect a radio luminosity of  $\sim 10^{30}\text{erg s}^{-1}(B_{pwn}/3\mu\text{G})^2$ . However a field  $> 10\mu\text{G}$  is required for those particles to emit above the ionospheric cutoff ( $\sim 30\text{MHz}$ ).

Another possible explanation of the extended emission is an exotic PWN, which might be powered by dissipation of magnetic field instead of the spin-down wind. One can try to estimate the value of the magnetic field at a typical distance from RRAT J1819–1548, of the order of the size of the nebula. This depends on the dynamics with which the magnetic field is advected outward: continuous outflow vs sporadic bursts.

For a smooth continuous outflow (either an unshocked flow, or for a strongly magnetized wind with a weak shock) the magnetic field at distances  $\sim R_{pwn}$ , is found supposing a magnetic dipole from the stellar surface ( $R_{psr}$ ) to the light cylinder ( $R_{lc}$ ) and then a monopolar solution up to  $R_{pwn}$ :

$$B(R_{pwn}) \approx B_{psr}(R_{psr}/R_{lc})^3(R_{lc}/R_{pwn}). \quad (5)$$

which gives  $B(R_{pwn}) \sim 0.5\mu\text{G}$ . This is a very small magnetic field, and as stated before particles at energy exceeding what is allowed by the pulsar voltage would be required to produce the observed X-ray emission. Moreover in a strongly magnetized outflow, only weak shocks are possible, and in this case shock acceleration is usually inefficient.

For a dynamical configuration, the nebular magnetic field might be provided by eruptive events related to fractures in the neutron star crust that take part of the magnetic energy stored in the neutron star and transfer it to the nebula. However for a bubble expanding adiabatically from a size of the order of the pulsar to a size of the order of the nebula the magnetic field should drop by a factor  $(R_{psr}/R_{pwn})^2$  (magnetic flux conservation). Even for the very high inferred field at the neutron star surface, the values that are obtained at the distance of the nebula are far too small.

The above arguments appear to tentatively disfavour the magnetically powered idea, not just in the case of RRAT J1819–1548, but as a general interpretation of extended X-ray emission around strongly magnetized neutron stars. It is not a problem of explaining the luminosity (energetic), but of explaining radiation in the X-ray band as due to synchrotron. Interestingly the magnetically powered idea could still work in the case of a Compton nebula, to energize the low energy relic electrons.

The third possibility we want to discuss is that of a scattering halo. Scattering of X-rays by interstellar dust on the line of sight produces a scattered halo around the point source (Draine 2003, and references therein). Therefore, for RRAT J1819–1458 there might be a possibility that we are looking at a scattering halo. However prediction of scattering by diffuse dust in the ISM give halo sizes  $\sim 10\text{arcmin}$ . Given the much smaller extension of the observed emission, reflection should be due to a local dust concentration around the source. We can estimate the flux of the halo using the method derived by Draine and Bond (2004) for direct determination of distances to nearby galaxies with bright background AGNs, QSOs, or GRBs (see

e.g. Rivera-Ingraham and van Kerkwijk 2010, for other examples of X-ray scattering halos). The flux of the scattered photons,  $I_{halo}$ , is related to the flux in the point source,  $I_{ptsrc}$ , by  $I_{ptsrc} = (I_{ptsrc} + I_{halo}) \exp(-\tau_{sca})$  (Draine 2003), where the total scattering optical depth,  $\tau_{sca}$ , may be determined using a model of interstellar dust consisting of a size distribution of carbonaceous and silicate grains:  $\tau_{sca}/A_V \approx 0.15 (E/\text{keV})^{-1.8}$  (Draine and Bond 2004). The optical extinction  $A_V$  may be obtained using the relation found by Predehl and Schmitt (1995) ( $A_V = 0.56 N_H [10^{21} \text{ cm}^{-2}] + 0.23$ ). For RRAT J1819–1458, using the parameters found in the present work (see Table 1) and the above equations, with  $E \sim 1 \text{ keV}$ , we obtain  $A_V \sim 3.6 \text{ mag}$ ,  $\tau_{sca} \sim 0.54$ ,  $I_{ptsrc} \sim 1 \times 10^{-13} \text{ erg cm}^{-2} \text{ s}^{-1}$ , and a  $I_{halo} \sim 0.3 \times 10^{-13} \text{ erg cm}^{-2} \text{ s}^{-1}$ . This flux of the halo is of the order of that observed for the extended X-ray emission (see Sect. 3.3.2).

This study has shown that the extended X-ray emission around RRAT J1819–1458, detected with a very high significance, if due to synchrotron requires a high efficiency of injection for the X-ray emitting particles, much higher than in young PWNe. If due to IC-CMB, it could trace a relic population of pairs injected during the life of the system. Either a PWN or a scattering halo are possible interpretations, while the magnetically powered scenario appears to be tentatively disfavoured in the case of synchrotron emission, while we cannot rule out that it can provide an energizing source in the case of a Compton nebula.

**Acknowledgments.** This work was supported by the grants AYA2009-07391 and SGR2009-811, as well as the Formosa program TW2010005 and iLINK program 2011-0303. NR is supported by a Ramon y Cajal research position in CSIC. PS acknowledges support from NASA Contract NAS8-03060. This work was supported by Chandra Observer Support Award GO1-12091X. This publication makes use of data products from the Two Micron All Sky Survey, which is a joint project of the University of Massachusetts and the Infrared Processing and Analysis Center/California Institute of Technology, funded by the National Aeronautics and Space Administration and the National Science Foundation.

## REFERENCES

- Bucciantini, N., Arons, J., and Amato, E.: 2011, *MNRAS* **410**, 381
- Dhillon, V. S., Keane, E. F., Marsh, T. R., Stappers, B. W., Copperwheat, C. M., Hickman, R. D. G., Jordan, C. A., Kerry, P., Kramer, M., Littlefair, S. P., Lyne, A. G., Mignani, R. P., and Shearer, A.: 2011, *MNRAS* **414**, 3627
- Draine, B. T.: 2003, *ApJ* **598**, 1026
- Draine, B. T. and Bond, N. A.: 2004, *ApJ* **617**, 987
- Esposito, P., Tiengo, A., Rea, N., and et al.: 2012, *MNRAS* *submitted*
- Kaplan, D. L., Esposito, P., Chatterjee, S., Possenti, A., McLaughlin, M. A., Camilo, F., Chakrabarty, D., and Slane, P. O.: 2009, *MNRAS* **400**, 1445
- Kargaltsev, O., Pavlov, G. G., and Durant, M.: 2012, *ArXiv e-prints*
- Keane, E. F. and McLaughlin, M. A.: 2011, *Bulletin of the Astronomical Society of India* **39**, 333
- Li, X.-H., Lu, F.-J., and Li, Z.: 2008, *ApJ* **682**, 1166
- Lyne, A. G., McLaughlin, M. A., Keane, E. F., Kramer, M., Espinoza, C. M., Stappers, B. W., Palliyaguru, N. T., and Miller, J.: 2009, *MNRAS* **400**, 1439
- McLaughlin, M. A., Lyne, A. G., Lorimer, D. R., Kramer, M., Faulkner, A. J., Manchester, R. N., Cordes, J. M., Camilo, F., Possenti, A., Stairs, I. H., Hobbs, G., D’Amico, N., Burgay, M., and O’Brien, J. T.: 2006, *Nature* **439**, 817
- McLaughlin, M. A., Rea, N., Gaensler, B. M., Chatterjee, S., Camilo, F., Kramer, M., Lorimer, D. R., Lyne, A. G., Israel, G. L., and Possenti, A.: 2007, *ApJ* **670**, 1307
- Olausen, S. A., Kaspi, V. M., Ng, C.-Y., Zhu, W. W., Dib, R., Gavriil, F. P., and Woods, P. M.: 2011, *ApJ* **742**, 4
- Pacini, F. and Salvati, M.: 1973, *ApJ* **186**, 249
- Predehl, P. and Schmitt, J. H. M. M.: 1995, *A&A* **293**, 889
- Rea, N., Curto, G. L., Testa, V., Israel, G. L., Possenti, A., McLaughlin, M., Camilo, F., Gaensler, B. M., and Burgay, M.: 2010, *MNRAS* **407**, 1887
- Rea, N., McLaughlin, M. A., Gaensler, B., Chatterjee, S., Camilo, F., Kramer, M., Lorimer, D. R., Lyne, A. G., Israel, G. L., and Possenti, A.: 2008, in C. Bassa, Z. Wang, A. Cumming, and V. M. Kaspi (eds.), *40 Years of Pulsars: Millisecond Pulsars, Magnetars and More*, Vol. 983 of *American Institute of Physics Conference Series*, pp 74–78
- Rea, N., McLaughlin, M. A., Gaensler, B. M., Slane, P. O., Stella, L., Reynolds, S. P., Burgay, M., Israel, G. L., Possenti, A., and Chatterjee, S.: 2009, *ApJ* **703**, L41
- Reynolds, S. P., Borkowski, K. J., Gaensler, B. M., Rea, N., McLaughlin, M., Possenti, A., Israel, G., Burgay, M., Camilo, F., Chatterjee, S., Kramer, M., Lyne, A., and Stairs, I.: 2006, *ApJ* **639**, L71
- Rivera-Ingraham, A. and van Kerkwijk, M. H.: 2010, *ApJ* **710**, 797
- Vink, J. and Bamba, A.: 2009, *ApJ* **707**, L148
- Younes, G., Kouveliotou, C., Kargaltsev, O., Pavlov, G. G., Gogus, E., and Wachter, S.: 2012, *ApJ*, *in press*, *arXiv:1206.3330*